JACS
JOURNAL OF THE AMERICAN CHEMICAL SOCIETY

ARTICLE

pubs.acs.org/JACS

Gas-Phase Reactions of the Bare Th^{2+} and U^{2+} Ions with Small Alkanes, CH_4, C_2H_6, and C_3H_8: Experimental and Theoretical Study of Elementary Organoactinide Chemistry

Emanuela Di Santo,[†] Marta Santos,[‡] Maria C. Michelini,[†,*] Joaquim Marçalo,[‡] Nino Russo,[†] and John K. Gibson[§,*]

[†]Dipartimento di Chimica, Università della Calabria, Via P. Bucci, Cubo 14 C, 87030 Arcavacata di Rende, Italy
[‡]Unidade de Ciências Químicas e Radiofarmacêuticas, Instituto Tecnológico e Nuclear, 2686-953 Sacavém, Portugal
[§]Chemical Sciences Division, Lawrence Berkeley National Laboratory, Berkeley, California 94720, United States

S *Supporting Information*

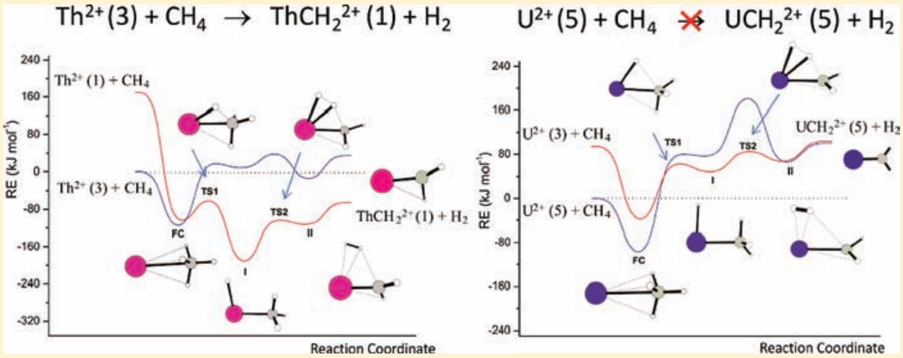

ABSTRACT: The gas-phase reactions of two dipositive actinide ions, Th^{2+} and U^{2+}, with CH_4, C_2H_6, and C_3H_8 were studied by both experiment and theory. Fourier transform ion cyclotron resonance mass spectrometry was employed to study the bimolecular ion—molecule reactions; the potential energy profiles (PEPs) for the reactions, both observed and nonobserved, were computed by density functional theory (DFT). The experiments revealed that Th^{2+} reacts with all three alkanes, including CH_4 to produce $ThCH_2^{2+}$, whereas U^{2+} reacts with C_2H_6 and C_3H_8, with different product distributions than for Th^{2+}. The comparative reactivities of Th^{2+} and U^{2+} toward CH_4 are well explained by the computed PEPs. The PEPs for the reactions with C_2H_6 effectively rationalize the observed reaction products, $ThC_2H_2^{2+}$ and $UC_2H_4^{2+}$. For C_3H_8 several reaction products were experimentally observed; these and additional potential reaction pathways were computed. The DFT results for the reactions with C_3H_8 are consistent with the observed reactions and the different products observed for Th^{2+} and U^{2+}; however, several exothermic products which emerge from energetically favorable PEPs were not experimentally observed. The comparison between experiment and theory reveals that DFT can effectively exclude unfavorable reaction pathways, due to energetic barriers and/or endothermic products, and can predict energetic differences in similar reaction pathways for different ions. However, and not surprisingly, a simple evaluation of the PEP features is insufficient to reliably exclude energetically favorable pathways. The computed PEPs, which all proceed by insertion, were used to evaluate the relationship between the energetics of the bare Th^{2+} and U^{2+} ions and the energies for C—H and C—C activation. It was found that the computed energetics for insertion are entirely consistent with the empirical model which relates insertion efficiency to the energy needed to promote the An^{2+} ion from its ground state to a prepared divalent state with two non-5f valence electrons ($6d^2$) suitable for bond formation in C—An^{2+}—H and C—An^{2+}—C activated intermediates.

INTRODUCTION

The first seminal studies of gas-phase actinide ion chemistry were performed by Armentrout et al., who studied the reaction of U^+ with nitrogen, hydrogen, and methane using an ion beam technique.[1] More recently, we have been engaged in studies of the gas-phase ion chemistry of the early actinides, An = Th, Pa, U, Np, Pu, Am, and Cm,[2−7] using Fourier transform ion cyclotron resonance mass spectrometry (FTICR-MS).[8] As was assessed in recent reviews,[9−11] prior to these studies, gas-phase ion chemistry experiments with highly radioactive members of the actinide series, Pa, Np, Pu, Am, Cm, Bk, Cf, and Es, had been based on the use of the laser ablation with prompt reaction and detection (LAPRD) technique, while FTICR-MS studies of An ions had been limited to Th and U. As FTICR-MS is well suited to extract kinetic and thermodynamic information from gas-phase reactivity studies, we have obtained new kinetic and thermochemical data for systems involving Pa,[6] Np,[2,4,5] Pu,[2,4] Am,[3,4] and Cm[7] by examining reactions of singly and doubly charged cations with oxidants. In addition to these recent studies of the reactivity of

Received: October 26, 2010
Published: January 25, 2011

dx.doi.org/10.1021/ja109621n | *J. Am. Chem. Soc.* 2011, 133, 1955–1970

An^{2+} ions with oxidants,[4,6,7] previous gas-phase experiments with An^{2+} ions have comprised reactions of U^{2+} with oxidants examined by FTICR-MS[12] and by quadrupole ion trap mass spectrometry (QIT-MS),[13] and reactions of Th^{2+} and U^{2+} with arenes studied by FTICR-MS.[14]

As in actinide chemistry in general, one of the questions raised by gas-phase reactivity studies is the possible participation of the 5f electrons of the early actinides in the observed chemistry. A potential way to probe the role of the 5f (and other valence electrons) is to study the gas-phase reactivity of An^{2+} ions with hydrocarbons: An^{2+} ions exhibit electronic configurations and energetics that can reveal the chemical activity of 5f electrons.[15] Alkanes and alkenes are suitable reaction substrates to establish correlations of the electronic configurations of the ions with reaction products and mechanisms, as demonstrated during the past two decades for (mainly singly charged) d-block and f-block metal cations.[16−20] The reactivity of singly charged actinide cations with alkanes and alkenes has been investigated previously by FTICR-MS (Th, U) and by time-of-flight mass spectrometry (TOF-MS) in an LAPRD setup (Th to Es).[9−11] Recently, we have used FTICR-MS to reinvestigate the reactivity of An$^+$ ions (An = Th to Cm) with alkanes and alkenes for a systematic comparison with the reactivity of AnO$^+$ ions (An = Th to Cm) with the same substrates;[21] particularly notable was the indication that the 5f electrons of Pa in PaO$^+$ are chemically active.

The gas-phase reactivity of doubly charged d-block metal cations with alkanes was examined with some detail by Freiser and co-workers 10−20 years ago,[22−32] following the seminal work by Tonkyn and Weisshaar[33,34] demonstrating that doubly charged d-transition-metal cations were not limited to electron transfer in their reactions with hydrocarbons; formation of doubly charged bond activation products, as well as H$^-$ or CH$_3^-$ transfer reactions, were observed along with electron transfer. A simple one-dimensional potential energy curve crossing model, derived from a Landau−Zener type of model, as first described by Spears et al.,[35] was successfully used by the groups of Weisshaar[33,34] and Freiser[22−32] to explain the observed reactivity patterns. In brief, at long range, the reactants, M^{2+} + RH, follow attractive ion-induced dipole potential energy curves, whereas the charged products of electron transfer, M$^+$ + RH$^+$, hydride transfer, MH$^+$ + R$^+$, or methide transfer, MCH$_3^+$ + (RH−CH$_3$)$^+$, follow repulsive Coulombic potential energy curves. The exothermicities of these reactions determine the curve crossing points and the products observed: if the reaction is not sufficiently exothermic and, consequently, the curve crossing distance is large, the transfer of an electron, a hydride, or a methide may not be feasible, and the M^{2+} ions can survive the crossing points to adequately short distances from the neutral to result in the formation of doubly charged products. This simplified model has been applied to varied systems involving doubly or, in general, multiply charged ions.[36−42] However, it has recently been pointed out that this model is an oversimplification in that some curve crossings do not actually exist because they occur along separate reaction coordinates.[43]

Freiser and co-workers studied the gas-phase reactivity of alkanes with transition-metal dipositive ions with d^1 (Sc^{2+},[32] Y^{2+},[32] La^{2+}[29]), d^2 (Zr^{2+}),[28] and d^3 (Nb^{2+},[22,24] Ta^{2+}[28]) ground-state electronic configurations (the core electrons are implicit) and a broad range of second ionization energies (11.1−16.2 eV). With these experiments, it was demonstrated that the d^1 metal ions had distinct reactivities relative to the d^2 and d^3 metal ions in terms of the formation of doubly charged products, and these differences were related to the occurrence of distinct reaction mechanisms.[32] Of particular interest is the proposed mechanism for alkane bond activation by M^{2+} ions with a d^1 configuration. As classical alkane activation by insertion—i.e., via generalized H−M^{2+}−C or C−M^{2+}−C types of intermediates—requires two valence bonding electrons at the metal center, activation by d^1 ions was rationalized by a generalized radical mechanism which proceeds by H-atom abstraction rather than formal insertion.[29] The reactivities of doubly charged lanthanide cations, Ln^{2+} (Ln = La, Ce, Pr, Nd, Sm, Eu, Gd, Tb, Dy, Ho, Er, Tm, Yb, Lu, that is, all Ln's except Pm), were subsequently studied with the same hydrocarbons, as well as with alkenes.[44] These Ln^{2+} ions possess “inert” 4f electrons, different accessibilities of d^1 electronic configurations, and a range of ionization energies,[45] such that these results provided a good basis for a refined comparison with the previous studies. The results for Ln^{2+} ion reactivity were essentially consistent with the model postulated by Freiser and co-workers, including the radical mechanism for activation of alkanes by d^1 M^{2+} ions.[44]

In a recent review of activation of alkanes by gas-phase metal ions,[42] Roithová and Schröder report on the plethora of theoretical studies of reactions of alkanes with monopositive metal ions and the corresponding dearth of such studies of reactions of alkanes with dipositive metal ions. A notable exception is the recent report of the reaction of Ta^{2+} with CH$_4$ studied both experimentally and by density functional theory (DFT).[43] We have been recently involved in the study of elementary gas-phase reactions of Th and U ions using DFT. These studies have examined the reactions of U$^+$ and U^{2+},[46] UO$^+$ and UO^{2+},[47] and Th$^+$ and Th^{2+} with H$_2$O,[48] of U$^+$ and U^{2+} with N$_2$O,[49] and of Th$^+$ and U$^+$ with CH$_4$[50] and C$_2$H$_6$.[51] Also recently, de Almeida and Duarte have reported DFT studies of the reactions of CH$_4$ with An$^+$ (An = Ac to Pu)[52] and with Th, Th$^+$, and Th^{2+}.[53]

In the present work, the gas-phase reactions of two dipositive actinide ions, Th^{2+} and U^{2+}, with small alkanes, CH$_4$, C$_2$H$_6$, and C$_3$H$_8$, were studied both experimentally and theoretically. These two actinides were chosen as the chemistry of thorium is essentially characteristic of a group 4 d-block transition element, whereas that of uranium is characteristic of an early 5f-block actinide element, with the possibility of chemically active 5f electrons. A central goal of this work is to determine if DFT can reliably model the reaction mechanisms of dipositive actinide ions with alkanes. As the applicability of DFT to reactions of alkanes with dipositive metal ions has received scant attention, the results provide a basis to evaluate the general applicability of DFT both to such reactions and to the special and particularly challenging actinides, where relativistic and other complicating many-electron effects come into play.[54]

■ EXPERIMENTAL METHODS

The experiments were performed in a Finnigan FT/MS 2001-DT FTICR mass spectrometer, equipped with a 3 T superconducting magnet, interfaced with a Spectra-Physics Quanta-Ray GCR-11 Nd:YAG laser operated at the fundamental wavelength (1064 nm), and controlled by a Finnigan Venus Odyssey data system.

The actinide samples were binary alloys of the actinide metal in a Pt matrix. These alloys were prepared by arc melting the An metal and Pt in water-cooled copper crucibles under Ti-gettered high-purity argon. The alloy compositions were ∼20 wt % natural Th (∼100% ^{232}Th) and depleted U (99.8% ^{238}U). The hydrocarbons, obtained from Air Liquide (>99.9% purity), were introduced into the spectrometer as supplied, through a leak valve, to pressures in the range of 3×10^{-8} to 2×10^{-7} Torr, and were checked in situ for their purity through electron ionization mass spectra. The neutral reagent pressures were measured with a Bayard−Alpert-type ionization gauge and calibrated using standard reactions of methane[55] and acetone[56] ions. The gauge readings were corrected for the relative sensitivities of the different reagents according to the approach of Bartmess and Georgiadis.[57]

Doubly charged actinide metal cations were produced by laser desorption/ionization (LDI) of the samples mounted on the solids probe of the spectrometer. Isolation of the An^{2+} ions was achieved using single-frequency, frequency sweep, or SWIFT excitation.[58] All ion manipulations and analyses were performed in the source cell of the dual-cell instrument.

The reactant ions were thermalized by collisions with argon, which was introduced into the spectrometer through pulsed valves to pressures of $\sim 10^{-5}$ Torr or through a leak valve to a constant pressure in the range of $(1-5) \times 10^{-6}$ Torr. The reproducibility of the reaction kinetics and the linearity of the semilog plots of normalized reactant ion intensities versus time indicated thermalization of the reactant ions. It should be noted that, in cases where excited electronic states react with kinetics similar to that of the ground state, linearity of semilog plots does not necessarily indicate complete thermalization; however, in such cases the interpretation of the results with reference to the thermalized component remains valid. When there was more than one product ion, reproducible product distributions for different collisional cooling periods or collision gas pressures also indicated that effective thermalization had been achieved. It is well-known that laser-ablated metal ions are produced with excess kinetic energies and can also be formed in electronically excited states.[59,60] For the actinides, the occurrence of strong spin−orbit coupling makes electronic relaxation less demanding than for d transition metals,[9] and therefore, collisional cooling of electronic excited states eventually formed in LDI is presumed to be a straightforward process. Collisional cooling as performed in the present study is also usually sufficient to remove any excess translational energy on the ions formed by LDI. In previous studies of the reactivity of singly charged[2,3,5,6,14,21] and doubly charged[4,6,7,12,14] An ions, performed under similar experimental conditions, no evidence was found for the involvement of excited states in the observed chemistry.

Rate constants, k, were determined from the pseudo-first-order decay of the relative signals of the reactant ions as a function of time at constant neutral pressures. The decays were followed until the relative intensity of the reacting dipositive ion had reached less than 10% of its initial intensity. For comparative purposes, reaction efficiencies are also reported as k/k_{COL}, where k_{COL} is the collisional rate constant derived from the modified variational transition-state/classical trajectory theory developed by Su and Chesnavich.[61] Collisional rate constants were calculated using experimental molecular polarizabilities of the hydrocarbons.[62] Due to uncertainties in the pressure measurements, we estimate errors up to ±50% in the absolute rate constants; however, relative errors are estimated to be ±20%.

In the reactions in which two singly charged products were generated, the product distributions were determined using the relative abundances of the metal-containing ions. The low-mass ions formed in these charge separation reactions showed rather low and variable intensities, most probably due to the high kinetic energies that they acquire,[30] which results in their loss from the ion trap. Conversely, the intensities of the high-mass metal-containing ions formed were observed to be reproducible, reflecting that these massive ions have relatively low kinetic energies.[30]

Care was taken to minimize the interference of reactions with residual water and oxygen present in the background of the mass spectrometer. This was accomplished by using long pumping periods after the solids probe was inserted into the high-vacuum chamber of the instrument but before introduction of the reagents. Base pressures in the turbomolecular-pumped spectrometer were typically $\sim 10^{-8}$ Torr. All the reactions were compared with reactions that occurred under background conditions. When the reactions with residual gases were significant, the measured reaction rates and product distributions were corrected for the presence of oxygenated products forming directly from the reactant metal ions.

■ COMPUTATIONAL DETAILS

Density functional theory in its three-parameter hybrid B3LYP[63,64] formulation was used together with the Stuttgart−Dresden basis set for the thorium and uranium atoms (25s16p15d7f)/[7s6p5d3f] in combination with the 60-core-electron[65] relativistic effective core potential (RECP). This small-core RECP, so-called SDD pseudopotential, replaces the 60 electrons in inner shells 1−4, leaving the explicit treatment of the $n = 5$ shell (5s, 5p, 5d, and 5f) and also the 6s, 6p, 6d, and 7s valence electrons. The 6-311++G(d,p) basis set of Pople and coworkers was employed for the rest of the atoms[66−68] (we refer to these results as B3LYP/SDD hereafter). These computations were carried out with the Gaussian 03 package.[69] Ultrafine (99 radial and 590 angular points) pruned grids for numerical integration were employed, as implemented in Gaussian 03. This computational approach was chosen on the basis of the performance observed in our previous studies of bare actinide cation reactivities.[46,48−51]

Singlet and triplet spin states were considered in all of the reactions involving Th^{2+} and quintet and triplet spin states in the case of U^{2+} reactions. Singlet-spin-state optimizations were done within the restricted Kohn−Sham formalism, whereas the open-shell structures were studied using spin-unrestricted methods. We have checked the $\langle S^2 \rangle$ values to evaluate whether spin contamination can influence the quality of the results. In all cases we have found that the calculated values differ from $S(S+1)$ by less than 5%.

No symmetry restrictions were imposed during the geometry optimizations, and we have employed several initial geometries for each of the studied species. The nature of the calculated stationary points was characterized by a vibrational analysis performed within the harmonic approximation. For all of the studied reactions we report potential energy profiles (PEPs) calculated as relative energies of the species involved in the reaction pathways with respect to the ground-state reactant asymptotes at 0 K. The zero-point vibrational energy (ZPVE) corrections were included in all of the relative energies.

We have ensured that every transition state has only one imaginary frequency and that the vibrational mode associated with the imaginary frequency corresponds to the correct movement of the involved atoms. All the minima connected by a given transition state were confirmed by performing IRC (intrinsic reaction coordinate) computations, as implemented in the Gaussian 03 program.[70,71]

The bonding properties of some key structures were studied using natural bond orbital (NBO) analysis.[72,73]

■ RESULTS AND DISCUSSION

The experimental results for the bimolecular reactions of Th^{2+} and U^{2+} with methane, ethane, and propane are summarized in Table 1 as measured reaction rate constants, reaction efficiencies expressed as observed rate constants relative to collisional rate constants, and product distributions. With the exception of U^{2+}/CH_4, for which no reaction is observed, the other five An^{2+}/C_mH_n reactions each proceed with moderate efficiencies in the range of $k/k_{COL} = 0.11-0.22$. The observed product distributions were quite disparate between Th^{2+} and U^{2+}, and a focus of the following discussion is on evaluating the observed reactivity differences on the basis of the computed PEPs.

As $IE[C_2H_6] = 11.0$ eV and $IE[C_3H_8] = 11.5$ eV[74] are both below $IE[Th^+] \approx 11.65$ eV and $IE[U^+] \approx 11.7$ eV,[75] electron transfer from these neutrals to An^{2+} is exothermic. The nonobservation of

Table 1. Product Distributions, Rate Constants (k), and Reaction Efficiencies (k/k_{COL}) for the Reactions of Th^{2+} and U^{2+} with CH_4, C_2H_6, and C_3H_8[a]

	CH_4			C_2H_6			C_3H_8		
An^{2+}	product	k	k/k_{COL}	product	k	k/k_{COL}	product	k	k/k_{COL}
Th^{2+}	$ThCH_2^{2+}$ (100)	0.22	0.11	$ThC_2H_2^{2+}$ (100)	0.28	0.15	$ThC_3H_4^{2+}$ (55) $ThC_2H_2^{2+}$ (35) $ThCH_3^{+}$ (10)	0.26	0.13
U^{2+}	no reaction	<0.001	<0.001	$UC_2H_4^{2+}$ (100)	0.34	0.18	$UC_3H_6^{2+}$ (40) $UC_2H_4^{2+}$ (15) UH^{+} (10) UCH_3^{+} (35)	0.42	0.22

[a] Product distributions (%) in parentheses. k in units of 10^{-9} cm^3 $molecule^{-1}$ s^{-1}.

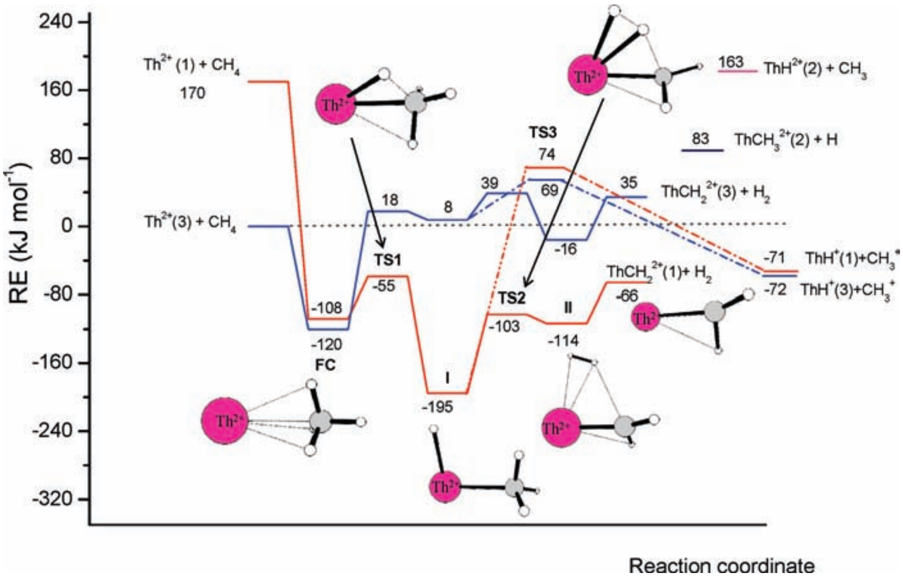

Figure 1. PEP for the reaction of $Th^{2+} + CH_4$ (triplet and singlet spin states) at the B3LYP/SDD level of theory. The labeling between the reactants and products identifies the first association complex (FC), the transition states (TS1, TS2, and TS3), and the intermediates (I and II). Spin states are given in parentheses. The geometrical parameters are given in Figure S1, Supporting Information.

these electron transfer channels can be attributed to the kinetic barrier discussed in the Introduction; a difference in IEs of at least 1 eV is generally required for electron transfer from a neutral to a dipositive ion.[30,44] As IE[CH_4] = 12.5 eV[74] exceeds IE[Th^+] and IE[U^+], electron transfer from CH_4 is endothermic and should not occur regardless of kinetic effects.

The general reaction pathways which were observed correspond to single and double dehydrogenation, methide transfer, and hydride transfer, as given by the following equations:

$$An^{2+} + C_mH_n \rightarrow AnC_mH_{n-2}{}^{2+} + H_2 \qquad (1)$$

$$An^{2+} + C_mH_n \rightarrow AnC_mH_{n-4}{}^{2+} + 2H_2 \qquad (2)$$

$$An^{2+} + C_mH_n \rightarrow AnCH_3{}^{+} + C_{m-1}H_{n-3}{}^{+} \qquad (3)$$

$$An^{2+} + C_mH_n \rightarrow AnH^{+} + C_mH_{n-1}{}^{+} \qquad (4)$$

The PEPs most pertinent to the observed reaction pathways are shown below; additional PEPs, as well as geometrical parameters, are provided in the Supporting Information.

Reactions with CH_4. As indicated in Table 1, methane is activated by Th^{2+} to produce the carbene, $ThCH_2^{2+}$, via elimination of H_2. In contrast, U^{2+} is inert toward methane to within the experimental detection limit. The computed PEPs for the Th^{2+}/CH_4 and U^{2+}/CH_4 reactions are shown in Figures 1 and 2. The geometrical parameters of all the species involved in these pathways are included as Supporting Information (Figures S1 and S2, respectively).

The reaction mechanism for the activation of CH_4 is similar to that reported for Th^+ and U^+,[50] as well as for other transition-metal ions.[43] The reaction starts with the insertion of the metal cation into the C−H bond of methane to form a hydrido−methyl intermediate, $H{-}An^{2+}{-}CH_3$ (intermediate I; An = Th, U). From that intermediate the H_2 elimination evolves through the formation of a four-centered transition state (TS2), which yields a second insertion intermediate $(H_2)An^{2+}{-}CH_2$ (II), in which the H_2 molecule is already formed. The last step of the reaction, formation of the dehydrogenation products, takes place directly from intermediate II, without an energy barrier. Other possible reaction products have been considered. In particular, the formation of AnH^+ and CH_3^+ products can be obtained by simple

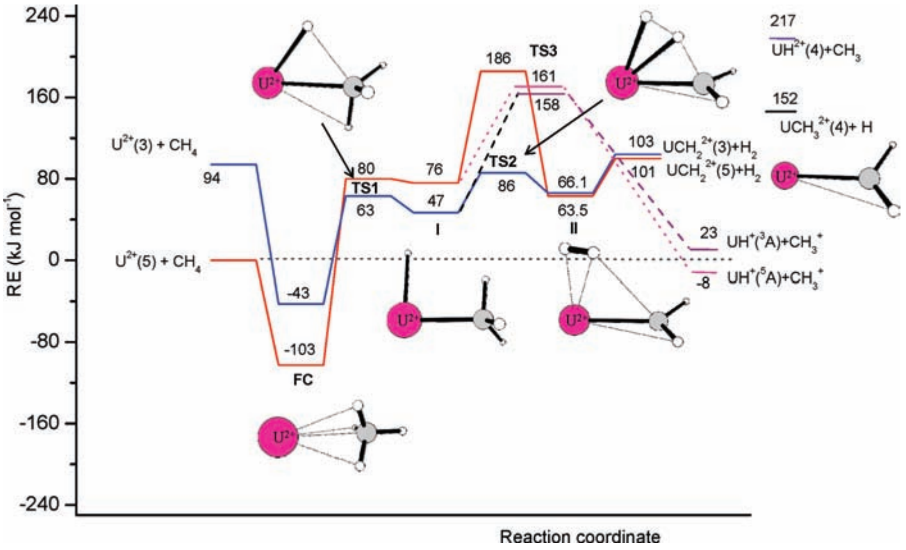

Figure 2. PEP for the reaction of $U^{2+} + CH_4$ (quintet and triplet spin states) at the B3LYP/SDD level of theory. The labeling between the reactants and products identifies the first association complex (FC), the transition states (TS1, TS2, and TS3), and the intermediates (I and II). Spin states are given in parentheses. The geometrical parameters are given in Figure S2, Supporting Information.

breaking of the An—C bond in the $H{-}An^{2+}{-}CH_3$ intermediate, after the surpassing of the associated activation barrier (TS3).

For Th^{2+}/CH_4, the two reactions given by the following equations are comparably exothermic, as indicated by the computed reaction energies (Figure 1):

$$Th^{2+} + CH_4 \rightarrow ThCH_2{}^{2+} + H_2 \qquad \Delta E = -66\ \text{kJ mol}^{-1} \tag{5}$$

$$Th^{2+} + CH_4 \rightarrow ThH^+ + CH_3{}^+ \qquad \Delta E = -72\ \text{kJ mol}^{-1} \tag{6}$$

Although the $CH_3{}^+$ elimination reaction is computed to be energetically competitive, only H_2 elimination is observed. Referring to the PEPs for eq 6 in Figure 1, it is apparent that the CH_3 elimination pathway is inhibited by transition states (TSs) which lie above the reactant energies and cannot be surmounted under the thermal conditions of the experiments (~298 K; $kT \approx 2.5$ kJ mol^{-1}). The very high TS energy barriers computed for this exothermic charge separation reaction are seen for other charge separation reactions studied in this work. As discussed above, the general observation of inefficient charge separation is consistent with the description of such reactions according to Landau—Zener theory, in which Coulombic repulsion of the two monopositive products presents an inherent barrier to such processes.[35] Referring to the PEP for Th^{2+}/CH_4, the very high energy TS3, which inhibits the exothermic formation of $ThH^+ + CH_3{}^+$, directly corresponds to the dissociation of $\{H{-}Th{-}CH_3\}^{2+}$ to the two monopositive products; the PEP computed by DFT evidently incorporates, at least qualitatively, the large barrier to the charge separation process.

For the Th^{2+}/CH_4 reaction, the H_2 elimination reaction proceeds with a moderate but significant efficiency, $k/k_{COL} = 0.11$. The computed PEP for this exothermic reaction (Figure 1) lies below the entrance energy, consistent with its observation. It is notable that the pathway for this reaction requires a spin crossing, from the triplet-state reactants to the singlet products. As is typical for actinide ion reactions, such spin crossing does not present an insurmountable barrier, presumably due to the enhanced spin—orbit coupling for these heavy atoms, which relaxes spin conservation restrictions. However, the necessity for spin crossing could account for the observed reaction efficiency of only 0.11. Several other spin crossing PEPs were computed for other observed reactions, as discussed below.

The computed PEP for the Th^{2+}/CH_4 reaction is in good agreement with the results recently obtained by de Almeida and Duarte for the same reaction using a similar computational approach.[53]

As shown in Figure 2, for U^{2+}/CH_4 the dehydrogenation reaction corresponding to eq 1 is computed to be substantially endothermic, in accord with the experimental observation that it does not occur. The $CH_3{}^+$ elimination channel corresponding to eq 2 is computed to be slightly exothermic; however, substantial barriers are encountered on the PEP, and this reaction is not expected to occur. The DFT results are in accord with the observed inert nature of U^{2+} toward CH_4.

Comparison of Figures 1 and 2 reveals that the association energies between the two An^{2+} ions and CH_4, i.e., the relative energy of the first complex, FC, are comparable: 120 kJ mol^{-1} for $Th^{2+}{-}CH_4$ and 103 kJ mol^{-1} for $U^{2+}{-}CH_4$. As this is primarily an electrostatic interaction, such agreement is expected. A key difference between the two PEPs is the much higher energy of TS1 and intermediate I for U^{2+}/CH_4 as compared with Th^{2+}/CH_4. This difference corresponds to a greater barrier to C—H bond insertion for U^{2+} and is in accord with empirical models which have related atomic energetics of metal ions with C—H (and C—C) bond activation efficiencies.[76] The correspondence between DFT and empirical models, evident for the An^{2+}/CH_4 reactions, also appears for other studied reactions, as elaborated below.

Reactions with C_2H_6. In contrast to CH_4, where U^{2+} is unreactive, with C_2H_6 both Th^{2+} and U^{2+} are reactive, with comparable efficiencies, 0.15 and 0.18, respectively. For Th^{2+} the sole product corresponds to double dehydrogenation, eq 7, whereas for U^{2+} only single dehydrogenation is observed, eq 8.

$$Th^{2+} + C_2H_6 \rightarrow ThC_2H_2{}^{2+} + 2H_2 \tag{7}$$

$$U^{2+} + C_2H_6 \rightarrow UC_2H_4{}^{2+} + H_2 \tag{8}$$

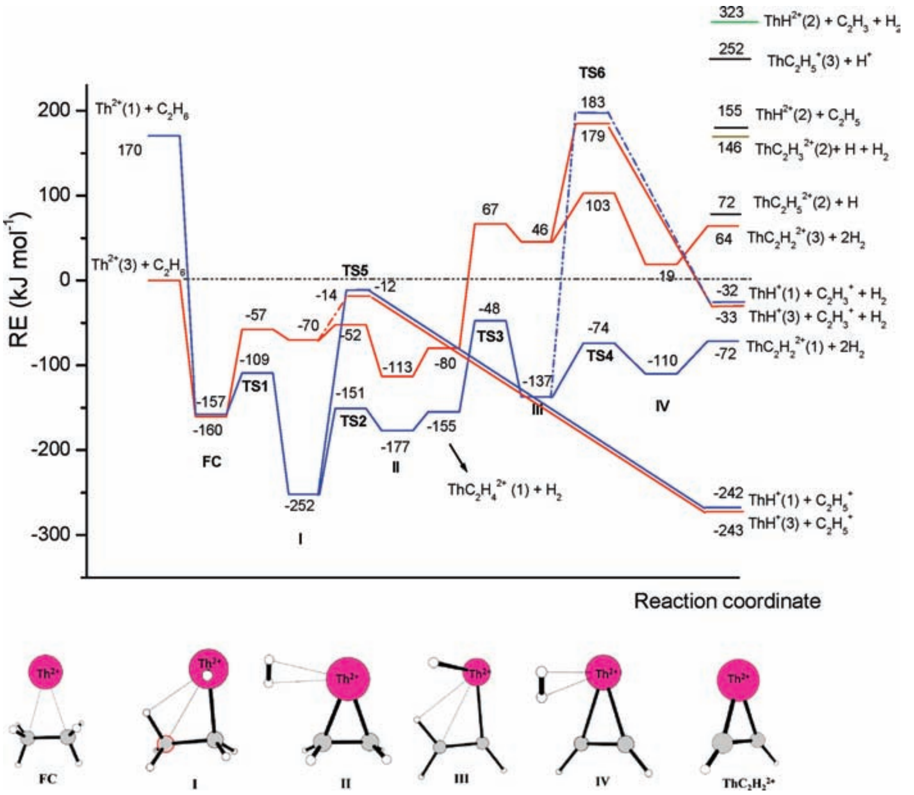

Figure 3. PEP for the first and second dehydrogenations of C_2H_6 by Th^{2+} (triplet and singlet spin states) at the B3LYP/SDD level of theory. The labeling between the reactants and products identifies the first association complex (FC), the transition states (TS1−TS6), and the intermediates (I−IV). Spin states are given in parentheses. The geometrical parameters for dehydrogenation are given in Figures S3 and S4, Supporting Information.

The PEP for the Th^{2+}/C_2H_6 dehydrogenation reaction is shown in Figure 3; the geometrical parameters of all the minima and transition states involved in the reaction are presented in Figures S3 and S4, Supporting Information. The reaction mechanism is similar to that described for the activation of CH_4. The double dehydrogenation process involves the formation of four different insertion intermediates, $H{-}Th^{2+}{-}C_2H_5$ (I), $(H_2){-}Th^{2+}{-}C_2H_4$ (II), $H{-}Th^{2+}{-}C_2H_3$ (III), and $(H_2)Th^{2+}{-}C_2H_2$ (IV), and the surmounting of the reaction barriers associated with each step (TS1 to TS4). The pathway for the first H_2 elimination involves a spin crossing from the triplet to singlet states to exothermically produce $\{ThC_2H_4^{2+} + H_2\}$. This reaction is sufficiently exothermic that the pathway to the second dehydrogenation lies below the entrance energy asymptote. The sequential elimination of two H_2 molecules to give $\{ThC_2H_2^{2+} + 2H_2\}$ is predicted by the PEP and is the only observed reaction.

The possibility of C−C activation of C_2H_6 by Th^{2+} was also considered, as shown in Figure 4. According to the PEP, the insertion of Th^{2+} into the C−C bond to give the very stable intermediate is accessible; the reaction pathway then proceeds to $\{ThCH_2^{2+} + CH_4\}$. The computed energy for this reaction channel indicates that it is substantially more exothermic than the observed double dehydrogenation channel. As seen in the PEPs in Figures 3 and 4, the initial association complex, FC, is identical for C−H and C−C activation at −160 kJ mol^{-1}. The subsequent barrier for C−H insertion, TS1 at −109 kJ mol^{-1}, is substantially lower than that for C−C insertion, TS1 at −60 kJ mol^{-1}. The reaction evidently proceeds from the initial association complex exclusively via the lower TS1, resulting solely in the observed double dehydrogenation. This reaction proceeds exclusively via the lower TS1, which would explain the preference for C−H activation though not the absence of the C−C activation channel.

The PEP for the U^{2+}/C_2H_6 dehydrogenation reaction is shown in Figure 5, and the corresponding optimized structures are given in Figures S6 and S7, Supporting Information. Assuming that the reaction proceeds along the lowest energy pathway, there is a crossing from the quintet reactants to the triplet pathway and then back to the quintet pathway to the $\{UC_2H_4 + H_2\}^{2+}$ single-dehydrogenation product, which is exothermic, albeit substantially less so than for Th^{2+}/C_2H_6. As the computed energy for TS1 in Figure 5, 4 kJ mol^{-1}, is slightly above the entrance energy, and TS2 is 16 kJ mol^{-1} above the entrance energy, the PEP predicts that this reaction should not proceed. Completely thermalized reactants in the FTICR-MS experiments possess 3/2 kT of relative translational energy and 3/2 kT of relative rotational energy and are thus at ~8 kJ mol^{-1} above zero. The rate-limiting TS2 barrier is thus ~8 kJ mol^{-1} above the reactant energy under the experimental conditions; we necessarily surmise that this latter value is within the uncertainty range of the computed transition-state energies. In contrast to the Th^{2+}/C_2H_6 reaction, the second dehydrogenation by U^{2+} is substantially endothermic, in accord with its nonobservation. The computed PEP for C−C activation of C_2H_6 by U^{2+} (Figure S8, Supporting Information) reveals that the reaction is endothermic and should not be observed. Assuming an uncertainty of at least ~8 kJ mol^{-1} in the computed TS2 for the reaction in Figure 5, which is a reasonable uncertainty at this level of theory, the DFT results are consistent with the distinctly exclusive double- and single-dehydrogenation products seen for Th^{2+} and U^{2+}, respectively, via classical C−H insertion mechanisms.

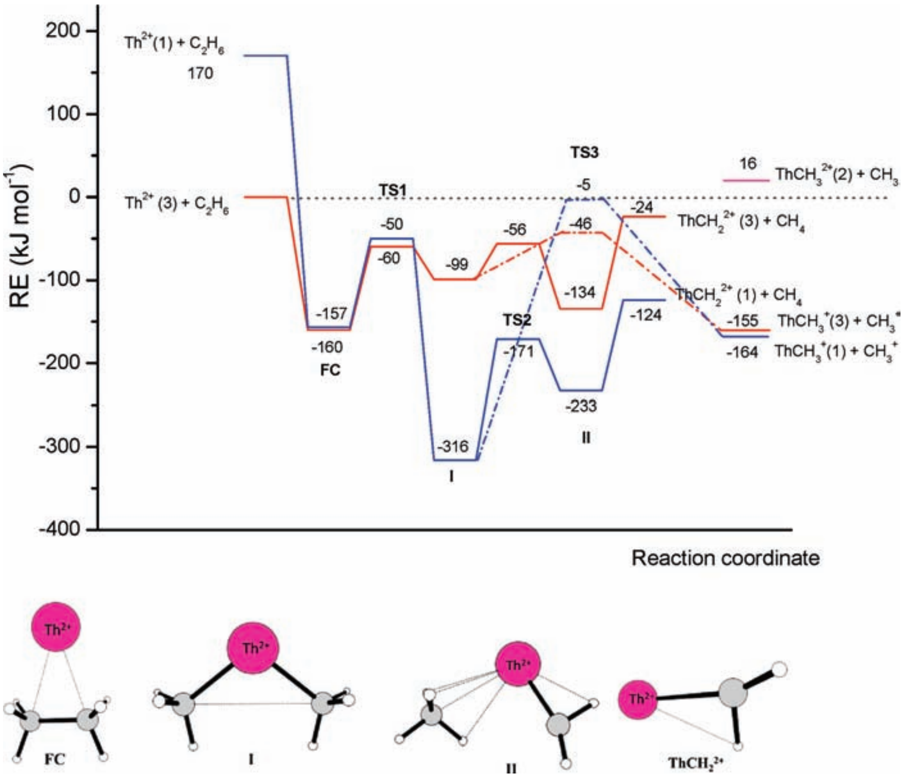

Figure 4. PEP for the C−C bond activation of C_2H_6 by Th^{2+} (triplet and singlet spin states) at the B3LYP/SDD level of theory. The labeling between the reactants and products identifies the first association complex (FC), the transition states (TS1, TS2, and TS3), and the intermediates (I and II). Spin states are given in parentheses. The geometrical parameters are given in Figure S5, Supporting Information.

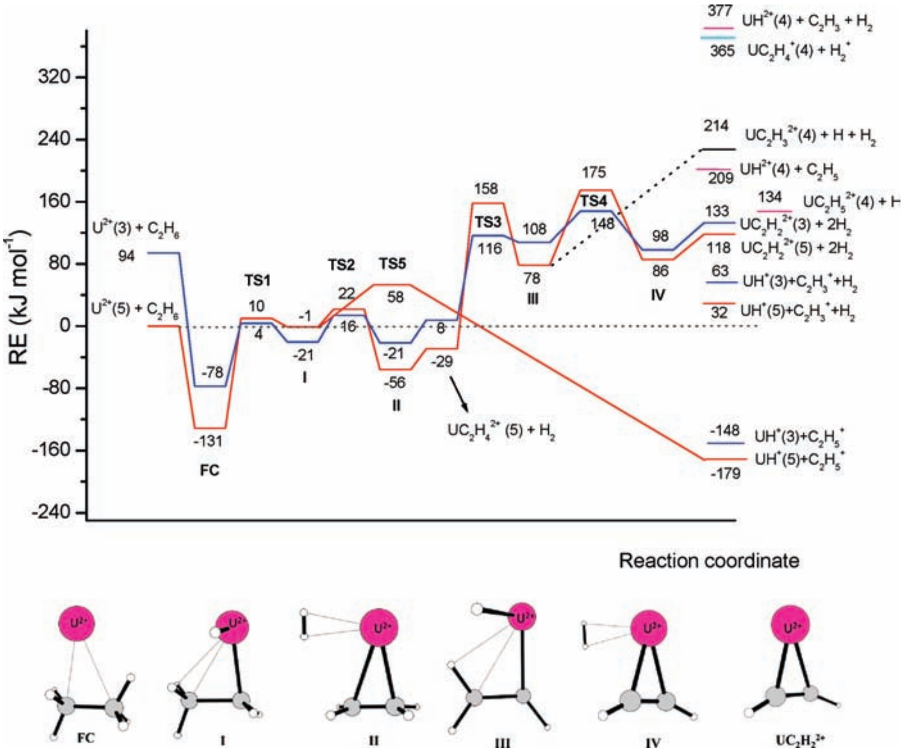

Figure 5. PEP for the first and second dehydrogenations of C_2H_6 by U^{2+} (quintet and triplet spin states) at the B3LYP/SDD level of theory. The labeling between the reactants and products identifies the first association complex (FC), the transition states (TS1−TS5), and the intermediates (I−IV). Spin states are given in parentheses. The geometrical parameters for dehydrogenation are given in Figures S6 and S7, Supporting Information.

A notable aspect of the $UC_2H_4^{2+}$ product is that the quintet spin state suggests that there are four nonbonding electrons at the uranium metal center, which would indicate that two covalent U−C bonds are not formed; triplet $UC_2H_4^{2+}$ lies 8 kJ mol^{-1} above the entrance energy, rendering it slightly endothermic. The computed geometry of quintet $UC_2H_4^{2+}$ (Figure S6, Supporting Information) is in concurrence with the qualitative bonding interpretation, particularly when compared with the geometry of singlet $ThC_2H_4^{2+}$ (Figure S3, Supporting Information). In the case of $UC_2H_4^{2+}$ (^{5}A) the U−C distance is 2.66 Å and the C−C distance is 1.37 Å. In contrast, for $ThC_2H_4^{2+}$ (^{1}A), the Th−C distance is 2.20 Å and the C−C distance is 1.60 Å. For comparison, the computed C−C distance in C_2H_6 is 1.53 Å and that in C_2H_4 is 1.33 Å. Whereas $ThC_2H_4^{2+}$ exhibits a structure indicative of a metallacycle with covalent Th−C bonds, the structure of $UC_2H_4^{2+}$ suggests that a much weaker electrostatic interaction of U^{2+} with the π-electron system of $H_2C{=}CH_2$ is occurring. To evaluate in greater detail the bonding in these species, NBO analyses were performed. Our calculations indicate that, in the case of $ThC_2H_4^{2+}$, the Th−C σ-bonds are formed from Th hybrid orbitals that have 50% d, 28% f, and 17% s character. The main contribution to these molecular orbitals is due to the C atoms (approximately sp^3 hybrids) with a polarization coefficient (0.89) that indicates that the Th−C bond can be described as a highly polarized covalent bond. NBO analysis describes the C−C bond as a single bond formed from sp^3 C hybrids. A similar analysis performed on the quintet $UC_2H_4^{2+}$ moiety indicates that there are no covalent bonds between the metal and the C atoms and there is a double bond between the C−C atoms. As expected, the σ-C−C bond is formed from sp^2 hybrids of C atoms, whereas the π-bond is formed from pure p C atomic orbitals.

The singlet $ThC_2H_2^{2+}$ ground-state geometry (Figure S4, Supporting Information) is characterized by a Th−C bond distance of 2.19 Å, a C−C bond distance of 1.36 Å, and a H−C−C angle of 129.8°. Accordingly, the NBO analysis predicts that a σ-bond is formed between the metal and each of the C atoms. These σ-bonds are formed from s−d−f metal hybrids (54% d, 25% f, and 20% s) with a very small contribution (2%) of p orbitals and sp^2 C hybrids. Again, the polarization coefficients (0.82 for C and 0.43 for Th) indicate that the covalent bonds are very polarized. In concurrence with the geometrical parameters, NBO indicates a double C−C bond.

In the case of the quintet ground-state $UC_2H_2^{2+}$ structure, the U−C bond distance (2.46 Å) is intermediate between that of $UC_2H_4^{2+}$ (2.66 Å) and the metal carbon distance in $ThC_2H_4^{2+}$ or $ThC_2H_2^{2+}$ (2.20 Å). The C−C bond (1.25 Å) is slightly shorter than that of $ThC_2H_2^{2+}$ (1.36 Å), whereas the H−C−C bond angle is slightly larger, 154.1° compared to the 129.8° of $ThC_2H_2^{2+}$. As suggested by the geometrical analysis, bond analysis indicates that there is some covalent bond formation between U and the C atoms in $UC_2H_2^{2+}$. However, these cannot be described as two full covalent bonds, similar to those formed in $ThC_2H_2^{2+}$. This structure is better described as a superposition of two Lewis structures in which the spin density is partially delocalized onto the C atoms (see Scheme 1 in the Supporting Information).

As is evident in Figures 3−5 and S8, Supporting Information, the charge separation reactions for Th^{2+} and U^{2+} with C_2H_6 to produce the corresponding $\{AnH^+ + C_2H_5^+\}$ or $\{AnCH_3^+ + CH_3^+\}$ are all substantially exothermic. However, for each of these reactions there is a high TS barrier which corresponds to the charge separation process and can be attributed to Coulombic repulsion between the nascent product ions, as discussed above. The case of the nonformation of $\{ThH^+ + C_2H_5^+\}$ is particularly illustrative as this reaction is substantially more exothermic than the observed double-dehydrogenation reaction and does not exhibit a TS which exceeds the entrance energy. As seen in Figure 3, the charge separation and dehydrogenation pathways diverge on the PEP after the insertion intermediate I: charge separation proceeds directly to the products via TS5, which lies at −14 kJ mol^{-1}, whereas dehydrogenation proceeds by hydrogen atom abstraction via TS2 at −151 kJ mol^{-1}. The absence of the charge separation channel is attributed to the much higher TS5 versus TS2 such that the reaction proceeds exclusively via the lower TS2 at this stage of the mechanism, which guides the reaction to the thermodynamically less stable products, $ThC_2H_2^{2+} + 2H_2$.

As with CH_4, the initial association complex energy wells, FC, are roughly comparable for Th^{2+} and U^{2+} at −160 and −131 kJ mol^{-1}, respectively. These association energies are somewhat greater for the more polarizable C_2H_6 molecule as compared with CH_4, as expected for a primarily electrostatic interaction.

Reactions with C_3H_8. The reactions of the An^{2+} ions with C_3H_8 are considerably more complex than with C_2H_6, from both the experimental and theoretical perspectives. As seen in Table 1, three products are observed with Th^{2+} and four with U^{2+}, as opposed to only one for C_2H_6 with both An^{2+} ions. To evaluate the experimental observations, many reaction pathways were evaluated by theory. For clarity, the discussion of the relationship between the experimental and theoretical results is focused on key points which establish that the computed PEPs are consistent with the observed reaction pathways. The seven experimentally observed reactions, reported in Table 1, are given by the following equations:

$$Th^{2+} + C_3H_8 \rightarrow ThC_3H_4^{2+} + 2H_2 \qquad (9)$$

$$Th^{2+} + C_3H_8 \rightarrow ThC_2H_2^{2+} + CH_4 + H_2 \qquad (10)$$

$$Th^{2+} + C_3H_8 \rightarrow ThCH_3^{+} + C_2H_5^{+} \qquad (11)$$

$$U^{2+} + C_3H_8 \rightarrow UC_3H_6^{2+} + H_2 \qquad (12)$$

$$U^{2+} + C_3H_8 \rightarrow UC_2H_4^{2+} + CH_4 \qquad (13)$$

$$U^{2+} + C_3H_8 \rightarrow UCH_3^{+} + C_2H_5^{+} \qquad (14)$$

$$U^{2+} + C_3H_8 \rightarrow UH^{+} + C_3H_7^{+} \qquad (15)$$

The only reaction pathway common to both Th^{2+} and U^{2+} is the formation of $\{AnCH_3^+ + C_2H_5^+\}$, eqs 11 and 14. The overall reaction efficiency of U^{2+}, k/k_{COL} = 0.22, is somewhat greater than that of Th^{2+}, k/k_{COL} = 0.13.

Figures 6 and 7 show the computed PEPs for dehydrogenation of C_3H_8 by Th^{2+} and U^{2+}, respectively. It is evident that the mechanisms are essentially identical; the primary difference is that the PEP for U^{2+} is shifted to higher energies after the first association complex, FC. This shift appears for the first intermediate complex, I, and is evidently related to the greater barrier for the initial insertion of U^{2+} into the C−H bond. The PEP for Th^{2+} proceeds to the highly exothermic single-dehydrogenation product, $ThC_3H_6^{2+}$, at −253 kJ mol^{-1}. In analogy with the Th^{2+}/C_2H_6 reaction, the Th^{2+} PEP continues on to the double-dehydrogenation product, with all of the transition-state energies

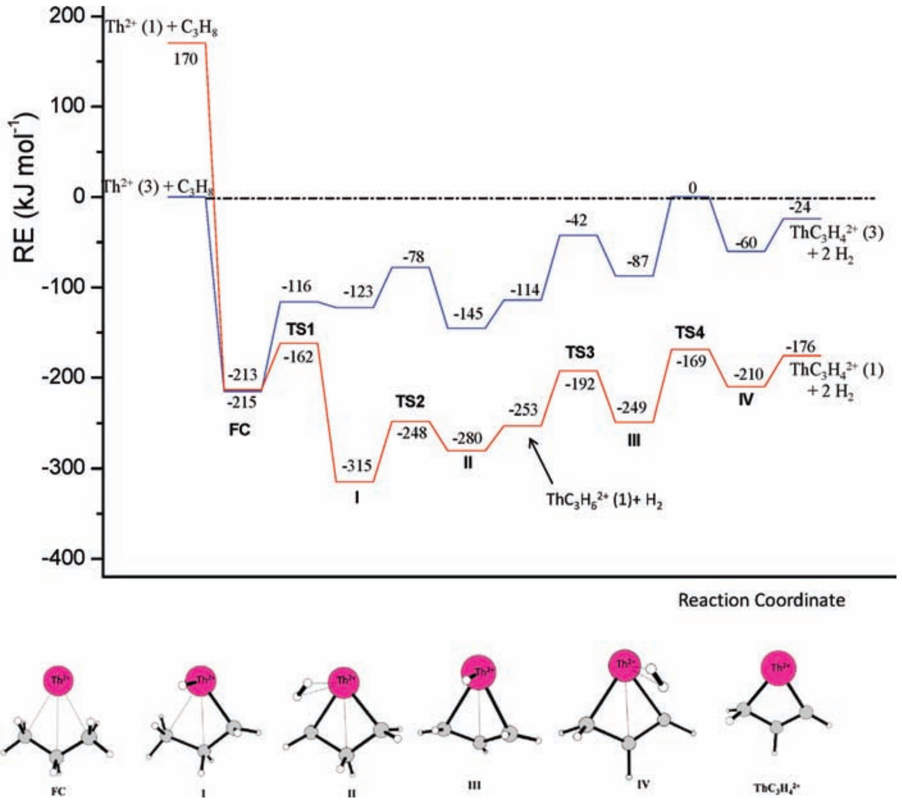

Figure 6. PEP for the first and second dehydrogenations of C_3H_8 by Th^{2+} (triplet and singlet spin states) at the B3LYP/SDD level of theory. The labeling between the reactants and products identifies the first association complex (FC), the transition states (TS1−TS4), and the intermediates (I−IV). Spin states are given in parentheses. The geometrical parameters are given in Figure S10, Supporting Information.

lying well below the entrance energy. The result is the considerably exothermic double dehydrogenation to give the product corresponding to eq 9. As seen in Figure 7, the corresponding PEP for U^{2+} proceeds below the entrance energy to the exothermic formation of $UC_3H_6^{2+}$, the observed dehydrogenation product. As with C_2H_6, the PEP then continues to endothermic double dehydrogenation, with transition states which lie well above the entrance energy. The computed PEPs are consistent with the observed double- and single-dehydrogenation reactions, eqs 9 and 12, for Th^{2+} and U^{2+}, respectively. Alternative PEPs for dehydrogenation of C_3H_8 by Th^{2+} and U^{2+} are shown in Figures S13 and S27, Supporting Information; these alternative pathways are consistent with the observed double and single dehydrogenations. These alternative PEPs differ from the dehydrogenation mechanism previously described in that the initial C−H bond activation occurs on a secondary C atom. Both dehydrogenation mechanisms are energetically very close. The first dehydrogenation products are slightly less exothermic in the case of Th^{2+} (−224 kJ/mol) and more exothermic in the case of U^{2+} (−100 kJ/mol). The double-dehydrogenation products are the same in both reaction mechanisms.

Figures 8 and 9 show the computed PEPs for the activation of a C−C bond leading to CH_4 elimination, followed by H_2 elimination, for Th^{2+} and U^{2+}, respectively. As for the case of C−H activation and double dehydrogenation, the two mechanisms are essentially the same. Again, the main difference is that the PEP for U^{2+} is shifted to substantially higher energies after the first association complex, FC, such that the insertion intermediate, I, lies at −315 kJ mol^{-1} for Th^{2+}, but at only −83 kJ mol^{-1} for U^{2+}. After the triplet to singlet spin crossing, the Th^{2+} PEP proceeds well below the entrance energy to the CH_4 elimination product at −231 kJ mol. This is followed by intramolecular C−H activation and ultimately exothermic H_2 elimination along a PEP which lies below the entrance energy. The predicted and observed overall reaction is as given by eq 10. In the corresponding case of U^{2+} (Figure 9), the C−C activation PEP proceeds to the observed exothermic CH_4 elimination product along a PEP which lies below the entrance energy. As for the U^{2+}/C_2H_6 PEP (Figure 5), there is double spin crossing, from quintet to triplet back to quintet, such that the product is $UC_2H_4^{2+}$ (^{5}A) discussed above, rather than $UC_2H_4^{+}$ (3) in which two of the four uranium valence electrons would be engaged in U−C covalent bonds. From the CH_4 elimination product, $UC_2H_4^{2+}$ (5), the U^{2+}/C_3H_8 reaction proceeds to intramolecular C−H activation and endothermic H_2 elimination along a PEP which lies above the entrance energy. It is evident from the computed PEPs why only CH_4 elimination is observed for U^{2+} (eq 13) whereas $\{CH_4 + H_2\}$ elimination is observed for Th^{2+} (eq 10). Alternative PEPs for $\{CH_4 + H_2\}$ elimination by Th^{2+} are shown in Figures S15 and S17, Supporting Information; these alternative pathways are consistent with eq 10; the high TS3 for H_2 elimination followed by CH_4 elimination (Figure S15) suggests initial CH_4 elimination by one or both of the favorable pathways shown in Figures 8 and S17. Alternative PEPs for $\{CH_4 + H_2\}$ elimination by U^{2+} are shown in Figures S29 and S31, Supporting Information; these alternative pathways are consistent with eq 13, the observation of CH_4 elimination without H_2 elimination.

The only reaction channel common to both Th^{2+} and U^{2+} is the methide abstraction charge separation to produce $\{AnCH_3^{+} + C_2H_5^{+}\}$, eqs 11 and 14; the respective PEPs are shown in

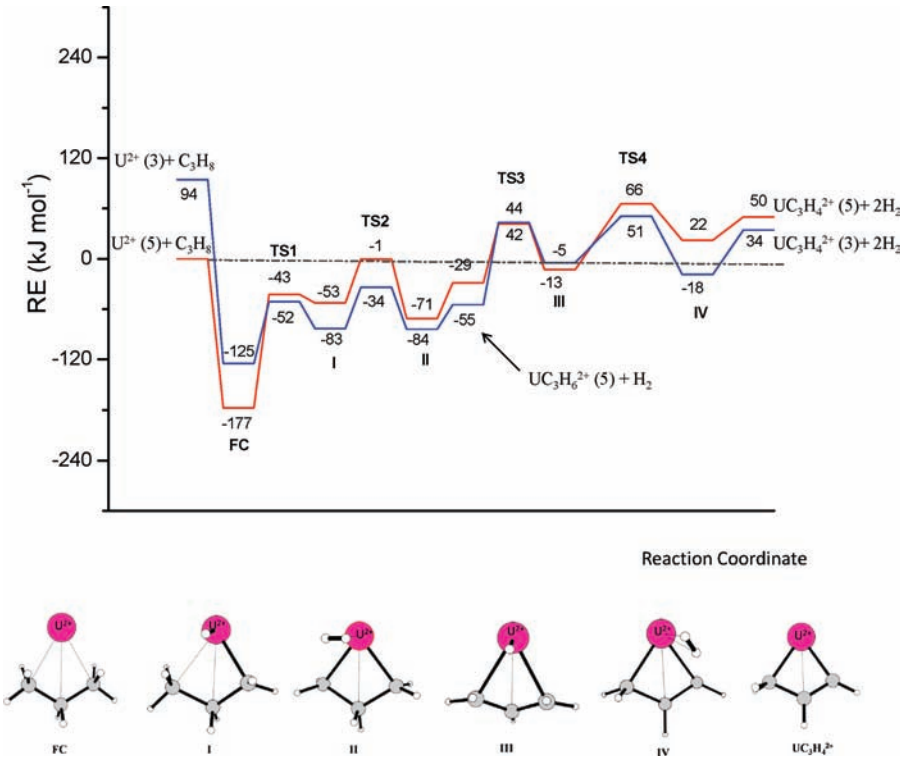

Figure 7. PEP for the first and second dehydrogenations of C_3H_8 by U^{2+} (quintet and triplet spin states) at the B3LYP/SDD level of theory. The labeling between the reactants and products identifies the first association complex (FC), the transition states (TS1−TS4), and the intermediates (I−IV). Spin states are given in parentheses. The geometrical parameters are given in Figure S23, Supporting Information.

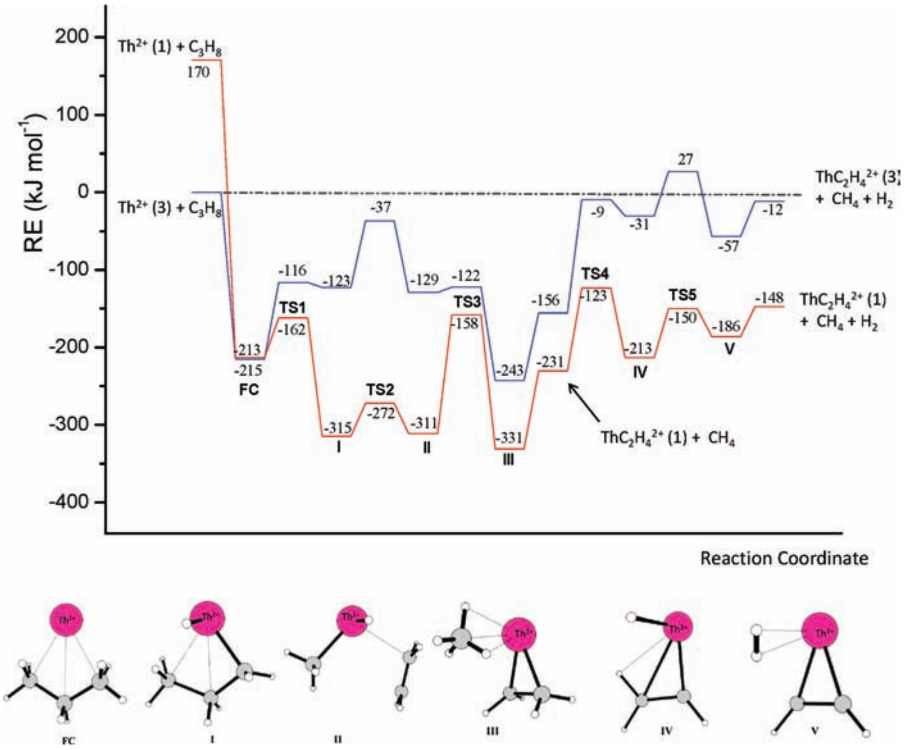

Figure 8. PEP for the elimination of CH_4 and H_2 from C_3H_8 by Th^{2+} (triplet and singlet spin states) at the B3LYP/SDD level of theory. The labeling between the reactants and products identifies the first association complex (FC), the transition states (TS1−TS5), and the intermediates (I−V). Spin states are given in parentheses. The geometrical parameters are given in Figure S11, Supporting Information.

Figures 10 and 11, respectively. For these reactions, the first association complexes, FC′, between An^{2+} and C_3H_8 do not engage all three carbon atoms and lie at slightly higher energies than the association complexes involved in the CH_4 elimination

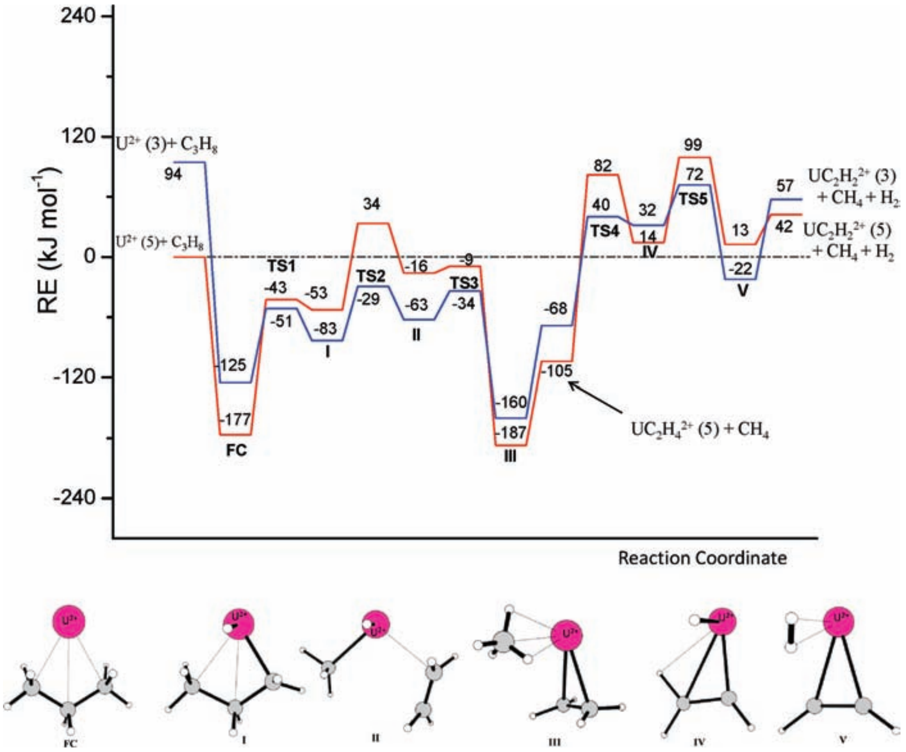

Figure 9. PEP for the elimination of CH_4 from C_3H_8 by U^{2+} (quintet and triplet spin states) at the B3LYP/SDD level of theory. The labeling between the reactants and products identifies the first association complex (FC), the transition states (TS1−TS5), and the intermediates (I−V). Spin states are given in parentheses. The geometrical parameters are given in Figure S24, Supporting Information.

PEPs in Figures 8 and 9; e.g., compare FC in Figure 8 and FC′ in Figure 10. Again, the PEPs for Th^{2+} and U^{2+} are similar, the primary difference being the typical shift of the PEP for U^{2+} to higher energies beginning at the first insertion intermediate, I. Both PEPs proceed below the entrance energy to the highly exothermic $\{AnCH_3^+ + C_2H_5^+\}$ products. The less exothermic $\{AnC_2H_5^+ + CH_3^+\}$ products are not experimentally observed.

The reaction of U^{2+} with C_3H_8 also proceeds to hydride abstraction, eq 15, as a minor channel. The PEP for this reaction (Figure 12) reveals that it is highly exothermic and proceeds below the entrance energy. As would be predicted by analogy with other reactions, the corresponding reaction for Th^{2+} should proceed along a similar PEP with a lower barrier to insertion and a more stable $\{H-Th-C_3H_7\}^{2+}$ insertion complex which can dissociate to the exothermic products $\{ThH^+ + C_3H_7^+\}$; the computed PEP for Th^{2+} (Figure S21, Supporting Information) indicates just this scenario. This is an example where it is evident that a computed PEP is consistent with an observed reaction, eq 15, whereas the corresponding computed PEP for another metal ion, here Th^{2+}, would be consistent with the occurrence of the analogous reaction, which is not observed. The experimental results suggest that the FC′ complexes between U^{2+} and C_3H_8 (Figures 11 and 12) are roughly 3 times more likely to proceed to C−C activation (Figure 11) rather than C−H activation (Figure 12), a result which would not be clearly predictable from the PEPs, specifically from the comparative TS1 barriers, which lie at −48 kJ mol^{-1} for C−C activation and at −68 kJ mol^{-1} for the less abundant C−H activation channel. It is evident that the computed PEPs are effective at identifying allowable reaction pathways and products, but cannot alone be employed to predict which allowable reaction pathways will predominate. These results illustrate the capabilities and limitations of considering the features of PEPs alone, such as well depths and barrier heights, for predicting and modeling reaction mechanisms. Deeper insights into the reaction mechanisms could be obtained by studying the motion of the atoms on the PES by means of molecular dynamics methodologies[77] or alternatively by simple RRKM calculations[78] or a phase space theory approach which incorporates angular momentum effects.[79]

Other computed PEPs are shown in Figures S19, S33, S35, and S37, Supporting Information. The only other potentially favorable computed reaction pathway was C_2H_6 elimination by Th^{2+} to exothermically produce $ThCH_2^{2+}$. However, the PEP for this reaction (Figure S19) exhibits a high TS1, only 16 kJ mol^{-1} below the entrance energy, and it is not surprising that this pathway is not experimentally observed.

Correlations between Computed Mechanisms and Atomic Energetics. In early studies of hydrocarbon activation by lanthanide cations it was found that there was a good correlation between the energy needed to excite the bare Ln^+ ions from their ground states to the lowest lying excited state with two non-4f valence electrons.[76] This observation indicated that the quasi-valence 4f electrons were ineffective at covalent bond formation, as is required in $C-Ln^+-H$ and $C-Ln^+-C$ activated intermediates. An analogous relationship was subsequently identified for the actinide ions, whereby the efficiencies of hydrocarbon activation processes parallel the energy needed to promote the An^+ ions from their ground electronic configuration to the lowest lying configuration with two non-5f valence electrons.[9] This latter observation indicated that for the actinide ions the 5f electrons are generally ineffective at covalent bond formation in hydrocarbon activation.

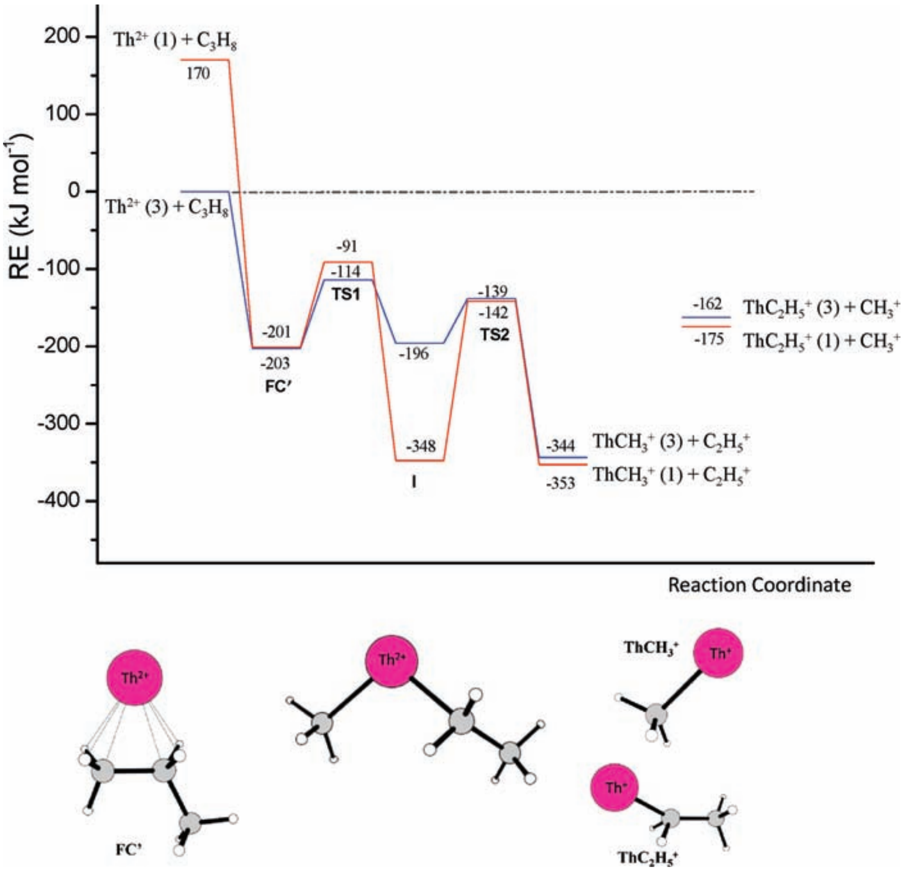

Figure 10. PEP for the elimination of $C_2H_5^+$ from C_3H_8 by Th^{2+} (triplet and singlet spin states) at the B3LYP/SDD level of theory. The labeling between the reactants and products identifies the first association complex (FC′), the transition states (TS1−TS2), and the intermediate (I). Spin states are given in parentheses. The geometrical parameters are given in Figure S12, Supporting Information.

For the dipositive lanthanide ions, the promotion energies to electronic configurations with two non-4f electrons are much higher than for the monopositive ions, and the observed reactivities toward small hydrocarbons have been attributed to the accessibility of the d^1 configurations and a radical reaction mechanism which does not involve direct insertion into a C−H or C−C bond.[44] The only Ln^{2+} ion which was found to (inefficiently) activate C_2H_6 and induce H_2 elimination was Gd^{2+}. The promotion energy for Gd^{2+} from its ground state, $4f^75d^1$, to the lowest lying configuration with two non-4f valence electrons, $4f^65d^2$, has been estimated as 930 ± 90 kJ mol^{-1};[80] this energy is prohibitively large to be accessible in an insertion reaction mechanism. Instead, the reactivity of Gd^{2+} was attributed to the ground-state d^1 configuration and the radical reaction mechanism postulated for d^1 transition-metal ions by Freiser and co-workers.[29,32]

A systematic study of reactions of the early monopositive actinide ions, Th^+ through Cm^+, with small alkanes was previously performed.[21] It was found that only Th^+ activated CH_4 and C_2H_6; as other An^+ ions, including U^+, with ground or low-lying electronic states with two non-5f electrons were unreactive, it is apparent that the monopositive An^+ ions are inherently less reactive toward alkanes as compared with the dipositive An^{2+} ions. It is instructive to compare our previous computational results for reactions of monopositive Th^+ and U^+ with CH_4[50] and C_2H_6[51] with the present results for the corresponding dipositive ions at the same level of theory, B3LYP/SDD. Of particular interest are the comparative depths of the energy wells for the initial FC association complexes, $An^{1+/2+}{-}C_xH_y$ (kJ mol^{-1}): $Th^+{-}CH_4$, −31; $U^+{-}CH_4$, −22; $Th^+{-}C_2H_6$, −33; $U^+{-}C_2H_6$, −19; $Th^{2+}{-}CH_4$, −120; $U^{2+}{-}CH_4$, −103; $Th^{2+}{-}C_2H_6$, −160; $U^{2+}{-}C_2H_6$, −131; $Th^{2+}{-}C_3H_8$, −215; $U^{2+}{-}C_3H_8$, −177. As expected, the association energy is substantially greater for the dipositive ions; these energies increase as the size and polarizability of the alkane increase. It would be expected that the additional energy provided to the reaction system for the dipositive ions could enable reaction mechanisms, such as insertion, which might not be feasible for a monopositive ion with otherwise similar electronic characteristics.

The first intermediate I for all of the computed reaction PEPs in this work corresponds to insertion of an An^{2+} ion into a C−H or a C−C bond to produce an activated intermediate. The reliability of empirical correlations of the efficiencies of such insertion mechanisms with the energy needed to promote the inserting actinide ion from its ground state to an excited state with two non-5f valence electrons suggests that the relative energies of the insertion complexes for Th^{2+} and U^{2+} should correlate with the promotion energies to a prepared divalent state suitable for insertion for these two ions. The energetics of the low-lying electronic configurations Th^{2+} and U^{2+} are known.[15] For both ions the lowest lying configuration with two non-5f electrons is $5f^{n-2}6d^2$ ($n = 2$ for Th^{2+}; $n = 4$ for U^{2+}). In the case of Th^{2+}, the ground state is $5f^16d^1$ and the $6d^2$ configuration is nearly degenerate at 1 kJ mol^{-1}; for U^{2+}, the ground state is $5f^4$, the $5f^36d^1$ configuration is 3 kJ mol^{-1} higher, and the $5f^26d^2$ configuration is at 232 kJ mol^{-1} above the ground state, where

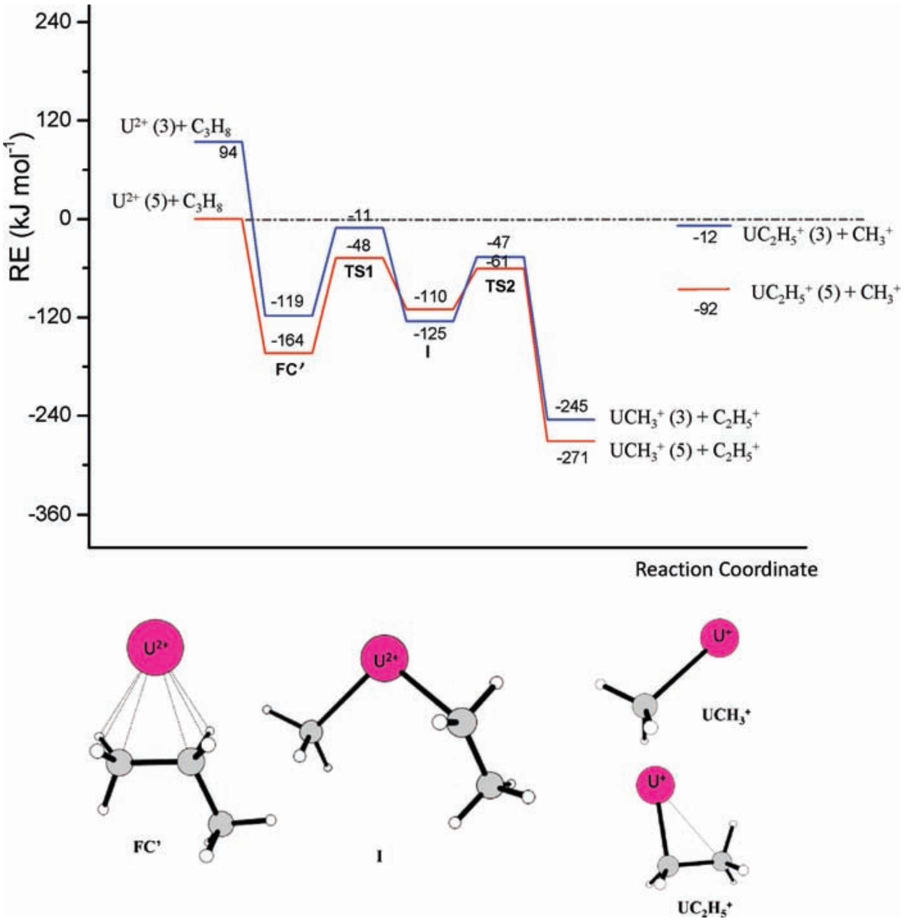

Figure 11. PEP for the elimination of $C_2H_5^+$ from C_3H_8 by U^{2+} (quintet and triplet spin states) at the B3LYP/SDD level of theory. The labeling between the reactants and products identifies the first association complex (FC′), the transition states (TS1−TS2), and the intermediate (I). Spin states are given in parentheses. The geometrical parameters are given in Figure S25, Supporting Information.

these energies correspond to the lowest spin−orbit level of the configuration. The $6d^1 7s^1$ configurations of Th^{2+} and U^{2+} are substantially higher in energy;[15,80] it is the $6d^2$ configuration which is considered important for effective insertion. According to the empirical promotion energy model, which presumes that a $6d^2$ configuration is necessary for insertion, it is predicted that the energy of the insertion should be approximately 230 kJ mol^{-1} less favorable for U^{2+} as compared with Th^{2+}. This proposed correlation can be evaluated from the computed PEPs for C−H and C−C activation; the results are compiled in Table 2. The computed insertion energies, ΔE_i, correspond to the difference in energy between the first association complex, FC, and the first insertion intermediate, I; the two C−C insertion energies given for C_3H_8 correspond to the two different first association complexes, FC and FC′, and insertion intermediates, I, which have different geometries. All of the insertion processes, FC → I, are substantially exothermic for Th^{2+}, from −75 kJ mol^{-1} for C−H activation in CH_4 down to −167 kJ mol^{-1} for C−C activation in C_3H_8. In contrast, all of the corresponding insertions are endothermic for U^{2+}, from +150 kJ mol for C−H activation in CH_4 down to +39 kJ mol^{-1} for C−C activation in C_3H_8. The differences between ΔE_i for Th^{2+} and U^{2+}, given in Table 2, are in the range of 184−261 kJ mol^{-1}. Although these differences are not unerringly at the predicted value of 230 kJ mol^{-1}, the results are clearly consistent with the correlation between promotion energies and insertion energies; as the electronic structures of the bare ions are perturbed by association and subsequent insertion, the consistent albeit nonexact agreement with the promotion energy model is quite remarkable. This evaluation of the PEPs demonstrates a direct relationship between electronic promotion energies of the bare Th^{2+} and U^{2+} ions and the computed DFT insertion energies and effectively validates the empirical promotion energy model which has been extensively and effectively employed to understand and predict the reactivities of bare lanthanide and actinide ions in the gas phase.

The shifts to higher energy of the entire PEPs for U^{2+} as compared with Th^{2+} due to the relative energies of the first insertion intermediates can essentially result in a shift from an exothermic to an endothermic reaction, as in the case of the reaction with CH_4 to produce $AnCH_2^{2+}$ ($+H_2$), which is exothermic for Th^{2+} but endothermic for U^{2+}. The PEP shift can alternatively result in different products for reactions which do proceed, as in the case of H_2 elimination from C_2H_6 by U^{2+} versus $2H_2$ elimination by Th^{2+}. A key implication of the evident necessity for formal promotion of ground-state U^{2+} from its $5f^4$ ground-state configuration to the $5f^2 6d^2$ configuration is that the unhybridized quasi-valence 5f electrons of uranium are not effective in covalent bond formation in C−H or C−C bond activation. It should be emphasized that this simplified picture is not entirely rigorous and that the NBO analysis indicates some 5f contribution to the bonding hybrid orbitals in the metal−hydrocarbon complexes.

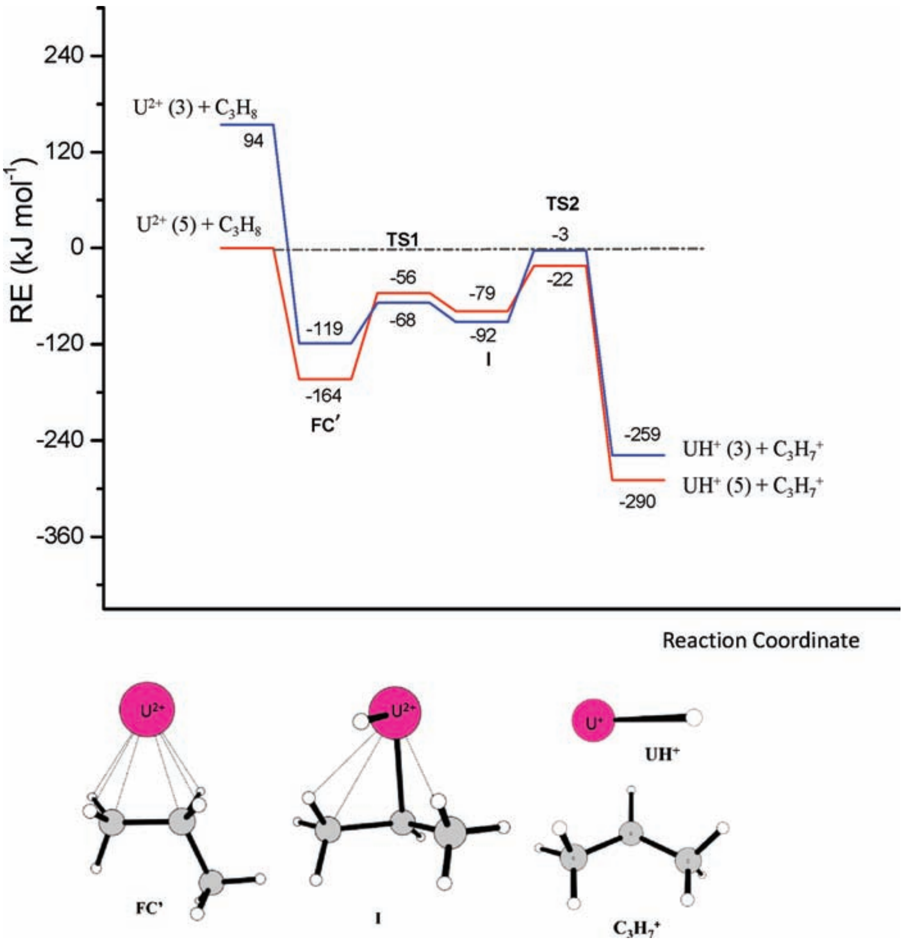

Figure 12. PEP for the elimination of $C_3H_7^+$ from C_3H_8 by U^{2+} (quintet and triplet spin states) at the B3LYP/SDD level of theory. The labeling between the reactants and products identifies the first association complex (FC′), the transition states (TS1−TS2), and the intermediate (I). Spin states are given in parentheses. The geometrical parameters are given in Figure S26, Supporting Information.

Table 2. Computed An^{2+} Insertion Energies for C−H and C−C Bond Activation[a]

C_mH_n	$\Delta E_i[Th^{2+}]$	$\Delta E_i[U^{2+}]$	$\Delta E_i[U^{2+}] - \Delta E_i[Th^{2+}]$
CH_4			
C−H[b]	−75	150	225
C_2H_6			
C−H[c]	−92	110	202
C−C[d]	−156	50	206
C_3H_8			
C−H[e]	−100	94	194
C−C[f]	−145	39	184
C−C[g]	−167	94	261

[a] $\Delta E_i[An^{2+}]$ is the energy difference, kJ mol^{-1}, between the first association complex, FC, and the insertion intermediate, I. [b] From Figures 1 and 2. [c] From Figures 3 and 5. [d] From Figures 4 and S8, Supporting Information. [e] From Figures 6 and 7. [f] From Figures 10 and 11. [g] From Figures S17 and S31, Supporting Information.

In a previous study of the reactivities of the dipositive lanthanide ions, Ln^{2+}, with alkanes and alkenes, the reactivity patterns indicated reactivity mechanisms associated with $5d^1$ electronic configurations.[44] These radical ion reactions were considered to proceed by H atom abstraction, rather than activation by insertion; the radical mechanism was first proposed by Freiser and co-workers.[29,32] The promotion energies for the Ln^{2+} from their ground states to the $5d^2$ configuration are much higher than the value of 232 kJ mol^{-1} for U^{2+}. Brewer has estimated that the lowest Ln^{2+} $5d^2$ configuration occurs for Ce^{2+}, which is known to lie 484 kJ mol^{-1} above the ground state.[80] It was previously found that Ce^{2+} is unreactive with C_2H_6 and only very inefficiently (k/k_{COL} = 0.007) dehydrogenates C_3H_8; in contrast, Gd^{2+}, which has a $5d^1$ ground state (but a very high promotion energy to the $5d^2$ configuration), dehydrogenates C_2H_6 and larger alkanes.[44] It is evident that the 484 kJ mol^{-1} promotion energy for Ce^{2+} is prohibitively large for alkane activation by insertion whereas the 232 kJ mol^{-1} promotion energy for U^{2+} is adequately low that activation by insertion proceeds for alkanes larger than CH_4. A promotion energy of 232 kJ mol^{-1} would render a monopositive f-block ion inert toward activation of small alkanes; the deeper energy well introduced by the interaction of the dipositive uranium ion with C_2H_6 and C_3H_8 surmounts the barrier to insertion. As the promotion energies to $6d^2$ for the dipositive transuranium actinide ions increase rapidly beyond U^{2+},[80] it is anticipated that activation by insertion will not proceed and that d^1 radical-type reactivity reminiscent of the Ln^{2+} ions will be observed.

■ CONCLUSIONS

A primary focus of this work was evaluating the ability of DFT to reliably model very elementary gas-phase organometallic reaction mechanisms. The dipositive actinide ions Th^{2+} and U^{2+} were of particular interest to test the efficacy of DFT for many-electron actinides, as well as for dipositive ions. The PEPs computed by DFT for the smallest alkanes were entirely consistent with the observations. The DFT results predict that Th^{2+} should activate CH_4 whereas U^{2+} should not, just as observed. For C_2H_6, DFT predicts that Th^{2+} should induce double dehydrogenation whereas U^{2+} should induce only single dehydrogenation, again as observed. The complexity increases drastically for the reactions with even the rather small alkane C_3H_8. The DFT results accurately predict several key aspects of the observed reaction pathways with C_3H_8: (1) double dehydrogenation for Th^{2+} and single dehydrogenation for U^{2+}; (2) $\{CH_4 + H_2\}$ elimination for Th^{2+} but only CH_4 elimination for U^{2+}; (3) $\{AnCH_3^+ + C_2H_5^+\}$ for both An = Th and An = U; (4) the favorable $\{UH^+ + C_3H_7^+\}$ reaction channel. However, the computed PEPs do not obviously predict certain features of the observed reaction pathways, such as why the favorable $\{ThH^+ + C_3H_7^+\}$ reaction channel is not observed, nor do the PEPs reliably predict branching ratios among the observed products. The ability of DFT to effectively model these reaction mechanisms has been clearly demonstrated; the nonobservation of pathways which are computed to be allowable is not whatsoever unexpected as these are not dynamic computations. The key result is that DFT effectively predicts allowable reaction pathways and that the experimental results—notably the significant differences between the products seen for Th^{2+} and U^{2+}—are entirely consistent with the computed PEPs.

All of the studied reactions were computed to proceed by initial insertion of the dipositive metal ion into either a C−H or a C−C bond. Evaluation of the DFT results in the context of elementary models used to understand such activation by f element ions revealed a close correspondence. Specifically, the energy required for the insertion of U^{2+} was consistently found to be greater than that for insertion of Th^{2+}, with insertion energy differences in the range of 185−261 kJ mol^{-1}. According to a hypothesis widely applied to reactions of monopositive lanthanide and actinide ions, if the quasi-valence f electrons are ineffective at covalent bond formation, and thus C−H or C−C bond activation, then promotion of the ion to a prepared divalent state with two non-f electrons is required for insertion. The non-5f divalent $6d^2$ configuration of Th^{2+} is nearly degenerate with the ground state, whereas the $6d^2$ configuration of U^{2+} lies 232 kJ mol^{-1} above its $5f^4$ ground-state configuration. The energy analysis of the computed PEPs thus indicates that the semiempirical promotion model is valid. Finally, it is evident that the observed reactivity of U^{2+} would not be observed for a monopositive ion with a comparable electronic configuration and promotion energy: the enhanced reactivity for the dipositive U^{2+} ion is attributed primarily to the greater energy of association of a dipositive ion with an alkane, as compared with the association energy for a monopositive ion.

■ ASSOCIATED CONTENT

Ⓢ **Supporting Information.** Complete ref 69, geometrical parameters for all of the minima and transition states in the reaction paths presented in Figures 1−12, alternative PEPs and associated geometrical parameters for observed reactions, and PEPs and associated geometrical parameters for nonobserved reactions. This material is available free of charge via the Internet at http://pubs.acs.org.

■ AUTHOR INFORMATION

Corresponding Author

mc.michelini@unical.it; jkgibson@lbl.gov

■ ACKNOWLEDGMENT

This work was supported by the Università degli Studi della Calabria, by FP7 Project HYPOMAP (Project 233482), by Fundação para a Ciência e a Tecnologia (FCT) under Contract PPCDT/QUI/58222/2004, and by the Director, Office of Science, Office of Basic Energy Sciences, Division of Chemical Sciences, Geosciences and Biosciences, of the U.S. Department of Energy at Lawrence Berkeley National Laboratory (LBNL) under Contract DE-AC02-05CH11231. The CINECA supercomputing center (Casalecchio di Reno, Italy) is gratefully acknowledged for providing computational resources. M.C.M. is grateful for the opportunity to be a Guest Scientist in the Chemical Sciences Division at LBNL. M.S. is grateful to FCT for a Ph.D. grant. We are grateful to Drs. António Pires de Matos and Richard G. Haire for their invaluable support in this project.

■ REFERENCES

(1) Armentrout, P. B.; Hodges, R. V.; Beauchamp, J. L. *J. Chem. Phys.* **1977**, *66*, 4683–4688.

(2) Santos, M.; Marçalo, J.; Pires de Matos, A.; Gibson, J. K.; Haire, R. G. *J. Phys. Chem. A* **2002**, *106*, 7190–7194.

(3) Santos, M.; Marçalo, J.; Leal, J. P.; Pires de Matos, A.; Gibson, J. K.; Haire, R. G. *Int. J. Mass Spectrom.* **2003**, *228*, 457–465.

(4) Gibson, J. K.; Haire, R. G.; Santos, M.; Marçalo, J.; Pires de Matos, A. *J. Phys. Chem. A* **2005**, *109*, 2768–2781.

(5) Gibson, J. K.; Haire, R. G.; Marçalo, J.; Santos, M.; Pires de Matos, A.; Leal, J. P. *J. Nucl. Mater.* **2005**, *344*, 24–29.

(6) Santos, M.; Pires de Matos, A.; Marçalo, J.; Gibson, J. K.; Haire, R. G.; Tyagi, R.; Pitzer, R. M. *J. Phys. Chem. A* **2006**, *110*, 5751–5759.

(7) Gibson, J. K.; Haire, R. G.; Santos, M.; Pires de Matos, A.; Marçalo, J. *J. Phys. Chem. A* **2008**, *112*, 11373–11381.

(8) Marshall, A. G.; Hendrickson, C. L.; Jackson, G. S. *Mass Spectrom. Rev.* **1998**, *17*, 1–35.

(9) Gibson, J. K. *Int. J. Mass Spectrom.* **2002**, *214*, 1–21.

(10) Gibson, J. K.; Marçalo, J. *Coord. Chem. Rev.* **2006**, *250*, 776–783.

(11) Heaven, M. C.; Gibson, J. K.; Marçalo, J. In *The Chemistry of the Actinide and Transactinide Elements*, 4th ed.; Morss, L. R., Edelstein, N. M., Fuger, J., Eds.; Springer: Dordrecht, The Netherlands, 2010; Vol. 6, Chapter 38.

(12) Cornehl, H. H.; Heinemann, C.; Marçalo, J.; Pires de Matos, A.; Schwarz, H. *Angew. Chem., Int. Ed. Engl.* **1996**, *35*, 891–894.

(13) Jackson, G. P.; King, F. L.; Goeringer, D. E.; Duckworth, D. C. *J. Phys. Chem. A* **2002**, *106*, 7788–7794.

(14) Marçalo, J.; Leal, J. P.; Pires de Matos, A.; Marshall, A. G. *Organometallics* **1997**, *16*, 4581–4588.

(15) Blaise, J.; Wyart, J.-F. *Energy Levels and Atomic Spectra of Actinides*; International Tables of Selected Constants, Vol. 20; Université Pierre et Marie Curie: Paris, 1992; http://www.lac.u-psud.fr/Database/Contents.html.

(16) Eller, K.; Schwarz, H. *Chem. Rev.* **1991**, *91*, 1121–1177.

(17) Armentrout, P. B. *Int. J. Mass Spectrom.* **2003**, *227*, 289–302.

(18) Operti, L.; Rabezzana, R. *Mass Spectrom. Rev.* **2006**, *25*, 483–513.

(19) Bohme, D. K. In *The Encyclopedia of Mass Spectrometry*; Gross, M. L., Caprioli, R., Eds.; Elsevier: New York, 2004; Vol. 4, pp 638−648.

(20) Roithová, J.; Schröder, D. *Chem. Rev.* **2010**, *110*, 1170–1211.

(21) Gibson, J. K.; Haire, R. G.; Marçalo, J.; Santos, M.; Pires de Matos, A.; Mrozik, M. K.; Pitzer, R. M.; Bursten, B. E. *Organometallics* **2007**, *26*, 3947–3956.

(22) Buckner, S. W.; Freiser, B. S. *J. Am. Chem. Soc.* **1987**, *109*, 1247–1248.

(23) Huang, Y.; Freiser, B. S. *J. Am. Chem. Soc.* **1988**, *110*, 4434–4435.

(24) Gord, J. R.; Freiser, B. S.; Buckner, S. W. *J. Chem. Phys.* **1989**, *91*, 7530–7536.

(25) Gord, J. R.; Freiser, B. S.; Buckner, S. W. *J. Chem. Phys.* **1991**, *94*, 4282–4290.

(26) Gord, J. R.; Freiser, B. S.; Buckner, S. W. *J. Phys. Chem.* **1991**, *95*, 8274–8279.

(27) Hill, Y. D.; Freiser, B. S.; Bauschlicher, C. W., Jr. *J. Am. Chem. Soc.* **1991**, *113*, 1507–1510.

(28) Ranasinghe, Y. A.; MacMahon, T. J.; Freiser, B. S. *J. Phys. Chem.* **1991**, *95*, 7721–7726.

(29) Ranasinghe, Y. A.; MacMahon, T. J.; Freiser, B. S. *J. Am. Chem. Soc.* **1992**, *114*, 9112–9118.

(30) Roth, L. M.; Freiser, B. S. *Mass Spectrom. Rev.* **1991**, *10*, 303–328.

(31) Freiser, B. S. *Acc. Chem. Res.* **1994**, *27*, 353–360.

(32) Hill, Y. D.; Huang, Y.; Ast, T.; Freiser, B. S. *Rapid Commun. Mass Spectrom.* **1997**, *11*, 149–154.

(33) Tonkyn, R.; Weisshaar, J. C. *J. Am. Chem. Soc.* **1986**, *108*, 7128–7130.

(34) Weisshaar, J. C. *Acc. Chem. Res.* **1993**, *26*, 213–219.

(35) Spears, K. G.; Fehsenfeld, G. C.; McFarland, M.; Ferguson, E. E. *J. Chem. Phys.* **1972**, *56*, 2562–2566.

(36) Bohme, D. K. *Int. Rev. Phys. Chem.* **1994**, *13*, 163–185.

(37) Herman, Z. *Int. Rev. Phys. Chem.* **1996**, *15*, 299–324.

(38) Schröder, D.; Schwarz, H. *J. Phys. Chem. A* **1999**, *103*, 7385–7394.

(39) Stace, A. J. *J. Phys. Chem. A* **2002**, *106*, 7993–8005.

(40) Price, S. D. *Phys. Chem. Chem. Phys.* **2003**, *5*, 1717–1729.

(41) Price, S. D. *Int. J. Mass Spectrom.* **2007**, *260*, 1–19.

(42) Roithová, J.; Schröder, D. *Phys. Chem. Chem. Phys.* **2007**, *9*, 2341–2349.

(43) Parke, L. G.; Hinton, C. S.; Armentrout, P. B. *J. Phys. Chem. A* **2008**, *112*, 10469–10480.

(44) Marçalo, J.; Santos, M.; Pires de Matos, A.; Gibson, J. K.; Haire, R. G. *J. Phys. Chem. A* **2008**, *112*, 12647–12656.

(45) Martin, W. C.; Zalubas, R.; Hagan, L. *Atomic Energy Levels—The Rare-Earth Elements*; U.S. National Bureau of Standards (NIST): Washington, DC, 1978.

(46) Michelini, M. C.; Russo, N.; Sicilia, E. *Angew. Chem., Int. Ed.* **2006**, *45*, 1095–1099.

(47) Michelini, M. C.; Russo, N.; Sicilia, E. *J. Am. Chem. Soc.* **2007**, *129*, 4229–4239.

(48) Mazzone, G.; Michelini, M. C.; Russo, N.; Sicilia, E. *Inorg. Chem.* **2008**, *47*, 2083–2088.

(49) Alikhani, M. E.; Michelini, M. C.; Russo, N.; Silvi, B. *J. Phys. Chem. A* **2008**, *112*, 12966–12974.

(50) Di Santo, E.; Michelini, M. C.; Russo, N. *Organometallics* **2009**, *28*, 3716–3726.

(51) Di Santo, E.; Michelini, M. C.; Russo, N. *J. Phys. Chem. A* **2009**, *113*, 14699–14705.

(52) de Almeida, K. J.; Duarte, H. A. *Organometallics* **2009**, *28*, 3203–3211.

(53) de Almeida, K. J.; Duarte, H. A. *Organometallics* **2010**, *29*, 3735–3745.

(54) Pepper, M.; Bursten, B. E. *Chem. Rev* **1991**, *91*, 719–741.

(55) Bruce, J. E.; Eyler, J. R. *J. Am. Soc. Mass Spectrom.* **1992**, *3*, 727–733.

(56) Lin, Y.; Ridge, D. P.; Munson, B. *Org. Mass Spectrom.* **1991**, *26*, 550–558.

(57) Bartmess, J. E.; Georgiadis, R. M. *Vacuum* **1983**, *33*, 149–153.

(58) Guan, S.; Marshall, A. G. *Int. J. Mass Spectrom. Ion Processes* **1996**, *157/158*, 5–37.

(59) Kang, H.; Beauchamp, J. L. *J. Phys. Chem.* **1985**, *89*, 3364–3367.

(60) Ibrahim, Y.; Alsharaeh, E.; Mabrouki, R.; Momoh, P.; Xie, E.; El-Shall, M. S. *J. Phys. Chem. A* **2008**, *112*, 1112–1124.

(61) Su, T.; Chesnavich, W. J. *J. Chem. Phys.* **1982**, *76*, 5183–5185.

(62) Lide, D. R., Ed. *CRC Handbook of Chemistry and Physics*, 88th ed.; CRC Press: Boca Raton, FL, 2007.

(63) Becke, A. D. *J. Chem. Phys.* **1993**, *98*, 5648–5652.

(64) Lee, C.; Yang, W.; Parr, R. G. *Phys. Rev. B* **1988**, *37*, 785–789.

(65) (a) http://www.theochem.unistuttgart.de/pseudopotentiale/. (b) Küchle, W.; Dolg, M.; Stoll, H.; Preuss, H. *J. Chem. Phys.* **1994**, *100*, 7535–7542.

(66) Krishnan, R.; Binkley, J. S.; Seeger, R.; Pople, J. A. *J. Chem. Phys.* **1980**, *72*, 650–654.

(67) Blaudeau, J. -P.; McGrath, M. P.; Curtiss, L. A.; Radom, L. *J. Chem. Phys.* **1997**, *107*, 5016–5021.

(68) Clark, T.; Chandrasekhar, J.; Schleyer, P. v. R. *J. Comput. Chem.* **1983**, *4*, 294–301.

(69) Frisch, M. J.; et al. *Gaussian 03*, revision C.02; Gaussian, Inc.: Wallingford, CT, 2004. See the Supporting Information for the complete reference.

(70) Gonzales, C.; Shlegel, H. B. *J. Chem. Phys.* **1989**, *90*, 2154–2161.

(71) Gonzales, C.; Shlegel, H. B. *J. Phys. Chem A* **1990**, *94*, 5523–5527.

(72) Reed, A. E.; Weinhold, F. *J. Chem. Phys.* **1985**, *83*, 1736–1740.

(73) Reed, A. E.; Curtiss, L. A.; Weinhold, F. *Chem. Rev.* **1988**, *88*, 899–926.

(74) Lias, S. G.; Bartmess, J. E.; Liebman, J. F.; Holmes, J. L.; Levin, R. D.; Mallard, W. G. *Gas-Phase Ion and Neutral Thermochemistry*; American Chemical Society: Washington, DC, 1988.

(75) Marçalo, J.; Gibson, J. K. *J. Phys. Chem. A* **2009**, *113*, 12599–12606.

(76) Cornehl, H. H.; Heinemann, C.; Schröder, D.; Schwarz, H. *Organometallics* **1995**, *14*, 992–999.

(77) Zhou, J.; Schlegel, H. B. *J. Phys. Chem. A* **2010**, *114*, 8613–8617.

(78) Ervin, K. M.; Armentrout, P. B. *J. Mass Spectrom.* **2004**, *39*, 1004–1015.

(79) Koizumi, H.; Armentrout, P. B. *J. Chem. Phys.* **2003**, *119*, 12819–12829.

(80) Brewer, L. *J. Opt. Soc. Am.* **1971**, *61*, 1666–1682.